New Journal of Physics
The open-access journal for physics

Precise quantum tomography of photon pairs with entangled orbital angular momentum

B Jack[1], J Leach[1], H Ritsch[2], S M Barnett[3], M J Padgett[1] and S Franke-Arnold[1,4]

[1] Department of Physics and Astronomy, SUPA, University of Glasgow, Glasgow, UK
[2] Institute of Theoretical Physics, University of Innsbruck, Austria
[3] Department of Physics, SUPA, University of Strathclyde, Glasgow, UK
E-mail: s.franke-arnold@physics.gla.ac.uk

New Journal of Physics **11** (2009) 103024 (12pp)
Received 29 May 2009
Published 12 October 2009
Online at http://www.njp.org/
doi:10.1088/1367-2630/11/10/103024

Abstract. We report a high fidelity tomographic reconstruction of the quantum state of photon pairs generated by parametric down-conversion with orbital angular momentum (OAM) entanglement. Our tomography method allows us to estimate an upper and lower bound for the entanglement between the down-converted photons. We investigate the two-dimensional state subspace defined by the OAM states $\pm\ell$ and superpositions thereof, with $\ell = 1, 2, \ldots, 30$. We find that the reconstructed density matrix, even for OAMs up to around $\ell = 20$, is close to that of a maximally entangled Bell state with a fidelity in the range between $F = 0.979$ and $F = 0.814$. This demonstrates that, although the single count-rate diminishes with increasing ℓ, entanglement persists in a large dimensional state space.

[4] Author to whom any correspondence should be addressed.

Contents

Entanglement is a defining feature of quantum mechanics associated with counter-intuitive non-classical correlations between separate parts of a quantum system [1]. Besides exhibiting one of the most striking failures of classical physics, entanglement has now become a valuable resource of quantum information technology and in particular quantum cryptography, where many protocols rely on strongly entangled states [2]. Therefore, the determination of the degree of entanglement contained in a given quantum state became an intense field of research [3]–[5]. In this context, a large number of measures to determine the degree of entanglement were proposed; these include negativity, tangle and entanglement of formation [6, 7]. In addition, EPR correlations [8] distinguish quantum entanglement from classical correlations in local realistic theories, a phenomenon that in its most stringent form is tested by violating Bell-type inequalities [9, 10].

Any quantum system is completely characterized by its density matrix, which thus predicts the outcome of any measurement. The density matrix of a bi-partite quantum system contains all information on the degree of entanglement. Hence, a measurement based reconstruction of the density matrix with sufficient fidelity is a viable method to characterize any possible system as a resource for quantum information processing [6, 11, 12]. This is usually a tedious experimental task but can be done by measurements of a suitable set of basis states.

In this paper, we determine the density matrix for twin photons generated by parametric down-conversion with respect to various subspaces of their orbital angular momentum (OAM) and angular position variables [13]. Related experiments by several groups have already investigated OAM correlations of down-converted photon pairs [11, 14, 15] and an uncertainty relation for orbital angular momentum and angle states has been tested experimentally [16]. Additionally, tomography of various superposition states in a three-dimensional (3D) OAM space have been demonstrated [17]. It is important to distinguish correlated measurement outcomes that may also arise for mixed quantum states [18] from quantum entanglement. We achieve this by reconstructing the complete density matrix of the two-photon system and evaluating its degree of entanglement [19]. By performing an overcomplete set of measurements, we can also determine an upper and lower bound of entanglement that is compatible with our measurements. The results demonstrate true quantum entanglement that cannot be mimicked by classical correlations. Note that precise tomographies of OAM states have been demonstrated successfully via Raman transitions in an atomic medium [20], recording the entanglement between an anti-Stokes photon and the atomic medium.

The OAM states of light constitute an infinitely dimensional Hilbert space with orthonormal basis states $|\ell\rangle$ characterized by an azimuthal phase factor $\exp(\mathrm{i}\ell\phi)$, carrying an OAM of $\ell\hbar$ per photon,

$$|\psi\rangle = \sum_{\ell=-\infty}^{\infty} a_\ell |\ell\rangle. \tag{1}$$

Constraining the states to a finite cut-off provides a practical testing ground for the implementation of qudits, which carry quantum information in a finite d-dimensional basis. In this paper, however, we restrict ourselves to 2D subsystems within the OAM basis states by selecting only a single pair of OAM-states $|\ell\rangle$ and $|-\ell\rangle$ for each photon, and superpositions thereof with $|\ell|$ reaching from 1 up to 30. This allows us to draw on tomographic methods developed for other 2D bi-partite systems as the polarization of light [6] or a metastable transition in trapped ion configurations [21]. While the process of parametric down-conversion becomes less efficient for higher order OAM modes [22], our measured density matrices show that entanglement still persists for OAM up to more than $|\ell| = 20$.

1. State tomography

Parametric down conversion generates photon pairs that, due to various conservation laws, are well correlated in space, time, frequency and polarization. The simultaneous entanglement of various degrees of freedom, or hyper-entanglement, has been observed experimentally [12]. Entanglement is also created in the OAM states as the total angular momentum of the incoming light is conserved [11, 23, 24], so that ideally the produced two-photon state is

$$|\Psi\rangle = \sum_{\ell=-\infty}^{\infty} a_{\ell,-\ell} |\ell\rangle|-\ell\rangle, \tag{2}$$

where $|a_{\ell,-\ell}|^2$ is proportional to the probability $P_{\ell,-\ell}$ to detect one photon in the state $|\ell\rangle$ and its partner photon in the state $|-\ell\rangle$. This may be understood by the required conservation of OAM in the down-conversion process.

Due to the decreasing overlap with the mode of the pump photon, the parametric down-conversion process becomes less efficient for the production of higher order OAM states. Experimentally we observe this as the decrease of the single counts as well as the coincidence counts with increasing $|\ell|$, shown in figure 1. All counts reported in this paper were measured for a time of 2 s times $|\ell|$ in order to allow for the decreasing efficiency.

The conjugate variable of OAM is the azimuthal angle [25]. Entanglement of the angular profile can be understood by considering superpositions of OAM states, which we term *angle states*. We define these in analogy to superpositions of polarization states as

$$|\alpha\rangle = \frac{1}{\sqrt{2}} \left(\mathrm{e}^{\mathrm{i}\alpha} |-\ell\rangle + \mathrm{e}^{-\mathrm{i}\alpha} |+\ell\rangle \right). \tag{3}$$

While the OAM states $|\ell\rangle$ are characterized by spiralling phase fronts, the angle states show a sinusoidal amplitude variation around the beam axis, proportional to $\sin(\ell\theta + \alpha)$. Angle states that differ by an angle of $\pi/2$ are orthogonal and provide an alternative basis set to the states $|\pm\ell\rangle$. Of particular interest to us are the states $|\alpha\rangle = |0\rangle$, $|\pi/2\rangle$, $|\pi/4\rangle$ and $|3\pi/4\rangle$, which in state space are analogous to the horizontal, vertical, diagonal and anti-diagonal polarization states, (see figure 2).

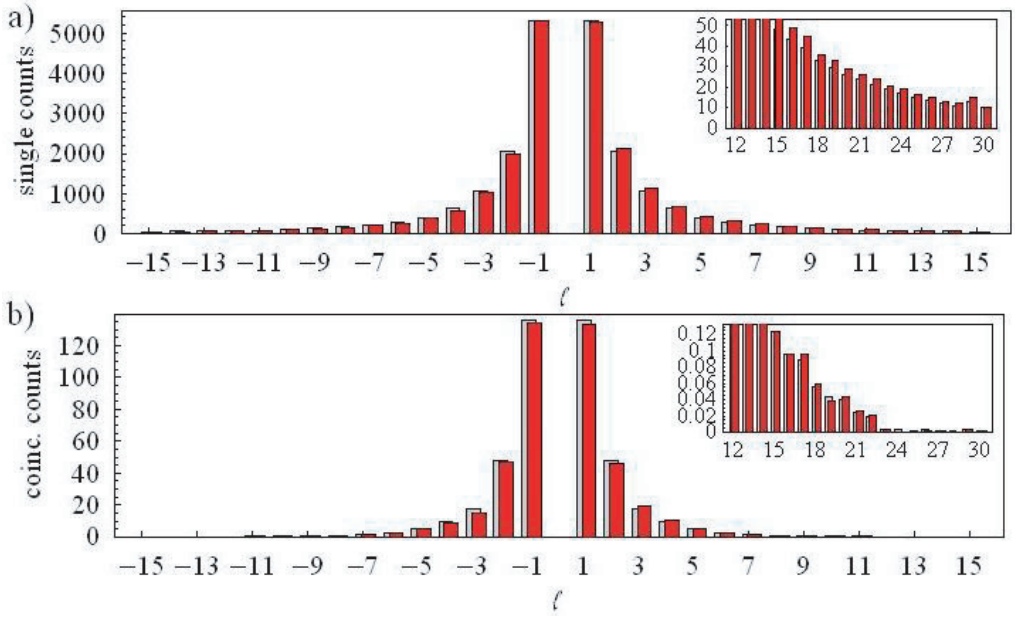

Figure 1. The generation of OAM modes tails off with increasing $|\ell|$. This can be seen both in the singles count rates (a) and the coincidence count rates (b). The red bars show the count rates proportional to $|a_{\ell,-\ell}|^2$, and the grey bars $(|a_{-\ell,-\ell}|^2 + |a_{\ell,-\ell}|^2 + |a_{-\ell,\ell}|^2 + |a_{\ell,\ell}|^2)/2$ for the coincidence counts and similarly for the single count rates. From the insets it is clear that the coincidence count rates become comparable to the noise level for $|\ell| > 22$.

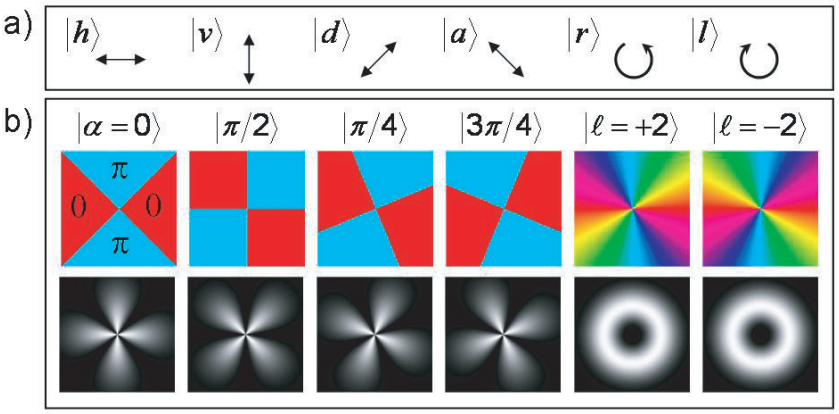

Figure 2. Different basis states describing the polarization of light (a) and the equivalent states for the OAM of light (b), here shown for the $|\ell| = 2$ subspace. Shown are the phase profiles (top) and intensity profiles (bottom).

By restricting ourselves to light within the subspace of $|\pm\ell\rangle$, from equation (2) we obtain an optimally entangled state

$$|\Psi\rangle = \frac{1}{\sqrt{2}}\left(|+\ell\rangle|-\ell\rangle + |-\ell\rangle|+\ell\rangle\right)$$
$$= \frac{1}{\sqrt{2}}\left(|\alpha\rangle|\alpha\rangle - |\alpha+\pi/2\rangle|\alpha+\pi/2\rangle\right), \quad (4)$$

meaning that photons are anti-correlated in their OAM, and correlated in their angular profile. Ideally a down-conversion source produces such entanglement, and we will compare our experiment with this ideal case.

Experimentally, the angle states $|\alpha\rangle$ (3) can be generated by passing light through an angular mask with a sinusoidal amplitude variation, $M = \sqrt{2}\cos\ell(\theta+\alpha)$, indicated in figure 2(b). The disadvantage of using such amplitude masks is their inherent loss. Alternatively, pure phase masks can be employed to approximate the angle states $|\alpha\rangle$ by reproducing the phase profile but with a uniform intensity distribution. We are using segment masks [26] that feature $2|\ell|$ sectors with alternating phases of zero and π which generate superpositions of mainly $\pm\ell$ with small sidebands at $\pm 3\ell, \pm 5\ell, \ldots$,

$$|\alpha\rangle \cong |\alpha_{\text{segment}}\rangle = \frac{2}{\pi}(e^{i\alpha}|-\ell\rangle + e^{-i\alpha}|\ell\rangle) + \frac{2}{3\pi}(e^{i\alpha}|-3\ell\rangle + e^{-i\alpha}|+3\ell\rangle) + \frac{2}{5\pi}(e^{i\alpha}|-5\ell\rangle + e^{-i\alpha}|+5\ell\rangle) + \cdots. \tag{5}$$

Light passes through such segment masks with a probability proportional to $|\langle\alpha_{\text{segment}}|\psi\rangle|^2$ with $|\psi\rangle$ from equation (2). Due to the finite spiral bandwidth of the down-converted light the coefficients a_ℓ of higher order OAM modes tail off quickly (compare figure 1) so that the segment masks effectively generate an excellent approximation to the angle states.

The eigenstates of the two qubit OAM density matrix may be expressed in terms of the OAM basis states $|\ell,\ell\rangle$, $|\ell,-\ell\rangle$, $|-\ell,\ell\rangle$, $|-\ell,-\ell\rangle$, which we will use in this paper. Any two qubit OAM density matrix can be written as

$$\rho = \begin{pmatrix} A_{11} & A_{12}e^{i\phi_{12}} & A_{13}e^{i\phi_{13}} & A_{14}e^{i\phi_{14}} \\ A_{12}e^{-i\phi_{12}} & A_{22} & A_{23}e^{i\phi_{23}} & A_{24}e^{i\phi_{24}} \\ A_{13}e^{-i\phi_{13}} & A_{23}e^{-i\phi_{23}} & A_{33} & A_{34}e^{i\phi_{34}} \\ A_{14}e^{i\phi_{14}} & A_{24}e^{i\phi_{24}} & A_{34}e^{i\phi_{34}} & A_{44} \end{pmatrix}, \tag{6}$$

where A_{ij} are the amplitudes and ϕ_{ij} the phases of the matrix elements. The diagonal elements of the density matrix describe the probability to detect simultaneously each of the twin photons in one of the states $|\ell\rangle$ and $|-\ell\rangle$. To determine the off-diagonal matrix elements requires measurements in superpositions of these states. We are reconstructing the density matrix from projection measurements onto the six (non-orthogonal) states $|\alpha=0\rangle$, $|\pi/2\rangle$, $|\pi/4\rangle$, $|3\pi/4\rangle$, $|+\ell\rangle$ and $|-\ell\rangle$. We measure the probability to find simultaneously each of the twin photons in one of these six states, yielding a total of 36 measurements, which are reported in the following section.

Each projection measurement can be expressed in terms of the density matrix elements ρ_{ij}, providing a set of 36 coupled equations to determine the 16 density matrix elements. In principle, a set of 16 measurements is sufficient if the corresponding transformation matrix is non-singular [6]. This procedure is favourable if a minimum number of potential measurements is required [27]. In our experimental set-up it is very easy to switch between different measurement states, so that we can take advantage of the information in all 36 measurements. This allows us to perform a least squares fit and the option to determine the largest and smallest degree of entanglement that is compatible with our measurements.

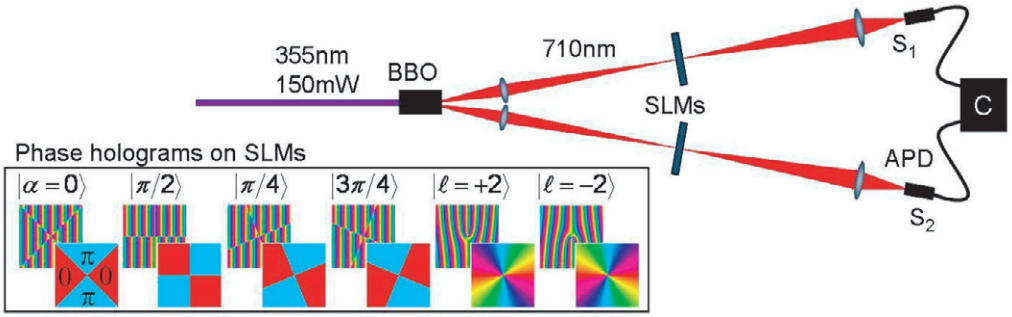

Figure 3. Experimental set-up. SLMs imaged onto avalanche photo detectors (APDs) allow us to perform projection measurements onto the six states $|0\rangle$, $|\pi/2\rangle$, $|\pi/4\rangle$, $|3\pi/4\rangle$, $|+2\rangle$ and $|-2\rangle$. We record single (S_1 and S_2) as well as coincidence counts (C).

2. Measurements

In our experiment we generate entangled photon pairs via a type I BBO crystal, cut for non-collinear phase matching with an external semi-cone angle of 4° (see figure 3). The crystal is pumped in normal incidence with a frequency-tripled, mode-locked Nd-YAG laser (Excyte) with an average power of 150 mW at 355 nm and a repetition rate of 100 MHz. Coincidences are recorded within a 25 ns window, so that there is a small chance that accidental correlations are recorded. These contribute to the background of our measurements. The spatial profile of the down-converted light is modified via spatial light modulators (SLMs) which are positioned in the image plane of the facet of the BBO crystal. We are using a Hamatsu LCOS SLM in reflection with a resolution of 600×800 pixels.

These computer-addressable diffractive elements transform light with the desired phase and amplitude profile into modes with a Gaussian profile that will couple into single mode fibres and be detected with avalanche photo diodes. Monitoring the correlations between the single counts allows us to filter out the entanglement present in all higher OAM modes.

In each channel of the down-converted photons, we cycle through six holograms that allow projection measurements onto the chosen basis states, recording both the signal count-rates S_1 and S_2 and the coincidence count-rate C. For determining the density matrix, we scale the measured coincidence count-rate with the single counts. This allows us to express a quantum contrast by $QC = C/(S_1 \times S_2)$, which gives the ratio of the coincidence counts over the classical (accidental) coincident counts $S_1 \times S_2$. These 36 projection measurements, depicted in figure 4 for the subspace $|\ell| = 3$ form the basis of the state tomography.

3. Reconstructing the density matrix

A physically allowed density matrix needs to fulfil certain criteria: its trace needs to be 1 and it must have non-negative eigenvalues, as they constitute true probabilities. This is not automatically guaranteed if we calculate the density matrix from measurements with finite precision. While the trace criterion can simply be corrected by proper normalization, other errors of the matrix obtained from the measurements like negative eigenvalues cause more problems. In fact, for a strongly entangled system being close to a pure state, for which one eigenvalue is

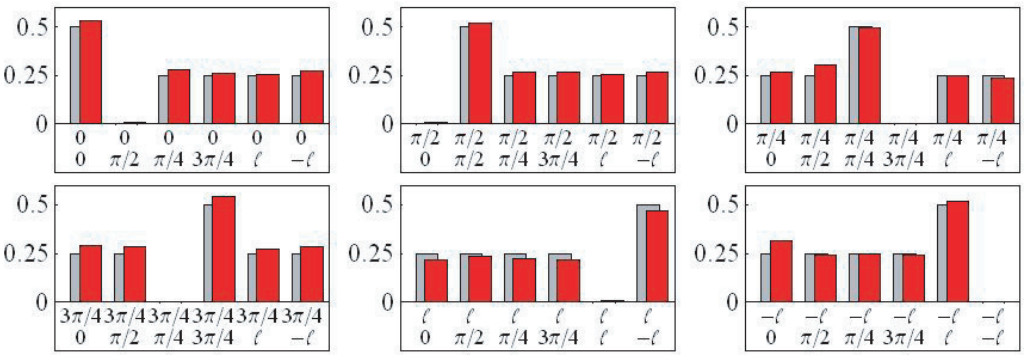

Figure 4. Characterization of the two-photon state by 36 correlation measurements of simultaneously detecting each photon in one of the six measurement states (red), and ideal values expected for a maximally entangled state and perfect measurements (grey). Shown are the results for the subspace $|\ell| = 3$.

typically close to one and all the others close to zero, such errors are particularly likely. This can be caused simply by noise, but it may also sometimes indicate contributions from additional states in a larger Hilbert space, which are not perfectly filtered out in the measurements. Various suggestions to cure this have been discussed in the literature [6, 29].

In this paper, we determine the density matrix that provides the best agreement with all our data, taking advantage of the over-complete set of $N = 36$ measurements for 16 unknowns. The most straightforward approach is to search numerically for the 10 independent amplitudes A_{ij} and the six phases ϕ_{ij} of the density matrix given in equation (6), which minimizes

$$\chi^2 = \sum_{i=1}^{36} \left(\frac{C_i^{(M)} - C_i^{(P)}}{\sqrt{C_i^{(M)} + 1}} \right)^2,$$

i.e. the difference between the count-rates predicted by the density matrix, $C^{(P)}$, and those recorded experimentally, $C^{(M)}$. This procedure does not necessarily result in a positive semi-definite matrix. We therefore explicitly enter the condition for positive eigenvalues as an additional constraint in the search algorithm. As an example, for the $|\ell| = 3$ subspace, this gives the density matrix with the minimum value of χ^2, shown in figure 5,

$$\rho = \begin{pmatrix} 0.008 & -0.027 & -0.026 & -0.003 \\ -0.027 & 0.457 & 0.484 & -0.005 \\ -0.026 & 0.484 & 0.530 & -0.004 \\ -0.003 & -0.005 & -0.004 & 0.004 \end{pmatrix} + i \begin{pmatrix} 0 & -0.002 & 0.000 & 0.004 \\ 0.002 & 0 & 0.012 & 0.000 \\ 0.000 & -0.012 & 0 & 0.002 \\ -0.004 & 0.000 & -0.002 & 0 \end{pmatrix}, \quad (7)$$

which has one large positive eigenvalue of 0.981, the three other eigenvalues being 0.013, 0.006 and 0.000. The sum of the squared eigenvalues is $\mathrm{Tr}(\rho^2) = 0.963$. The large first eigenvalue, indicative of a Bell state, shows that our system is almost a pure entangled state. While our χ^2 minimization procedure gives a valid density matrix, other, slightly differing forms also lie within the confidence limits. For a system such as ours which exhibits shot noise one would

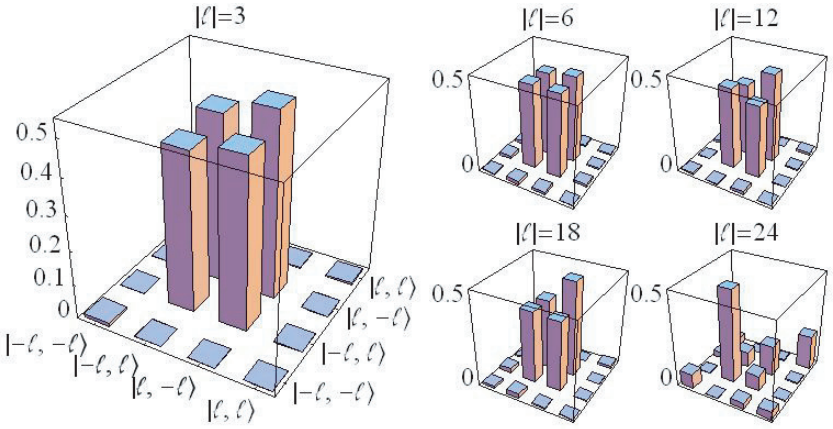

Figure 5. Graphical representation of the real part of the density matrix for various $|\ell|$ subspaces. For subspaces of $|\ell| \leqslant 22$ the four central entries of the density matrix dominate, indicating quantum entanglement. For larger ℓ the coincidence counts become comparable to the noise background and quantum correlations deteriorate.

anticipate that $\chi^2/N \simeq 1$. More precisely, one would expect χ^2 to lie in the range $N \pm \sqrt{2N}$ [28]. Within this range of possible χ^2, we use a secondary criterion to find the density matrix yielding the maximum or minimum entanglement that is consistent with our measurements, thereby establishing confidence limits for the degree of entanglement itself.

In practice, for subspaces where the total counts are high, the statistical uncertainty is very low and even when minimized, the value of χ^2 fails to fall below the upper bound of the $N \pm \sqrt{2N}$ range. We surmise that in these situations, the fidelity of our experiment is degraded by systematic noise sources such as alignment errors. In these cases, we simply take the χ^2 minimized matrix as the optimum solution. For subspaces where the overall count-rates are lower, the random statistical noise becomes dominant and χ^2 can be reduced below the upper bound. It is in these cases that we can identify possible density matrices that yield the largest or smallest degree of entanglement (in terms of ρ^2). As one might expect, in the cases of extremely low count-rates measurements are statistically compatible with both large and no entanglement.

4. State tomography

The reconstructed density matrices completely describe the generated two-photon state in the different OAM subspaces. Ideally we expect the Bell state described in (4), which is a pure and maximally entangled state. Imperfect phase-matching conditions during down-conversion as well as the presence of statistical noise in the detection system will deteriorate the state quality, and we find that especially for larger OAM subspaces with small single count-rates the state is no longer a pure state. The linear entropy, $SL = \frac{4}{3}(1 - \mathrm{Tr}(\rho^2))$ quantifies the mixture of the measured state [30], with a pure state being characterized by a linear entropy of zero, and a completely mixed state by $SL = 1$. We find that the state for low OAM subspaces is close to a pure state. For OAM subspaces from $|\ell| = 1$ to 20, we find values between $SL = 0.050$ and $SL = 0.350$ (see figure 6(a)). Photons generated with a higher OAM are found in an increasingly mixed state. The reason for this may be inherent to the down-conversion process itself, however

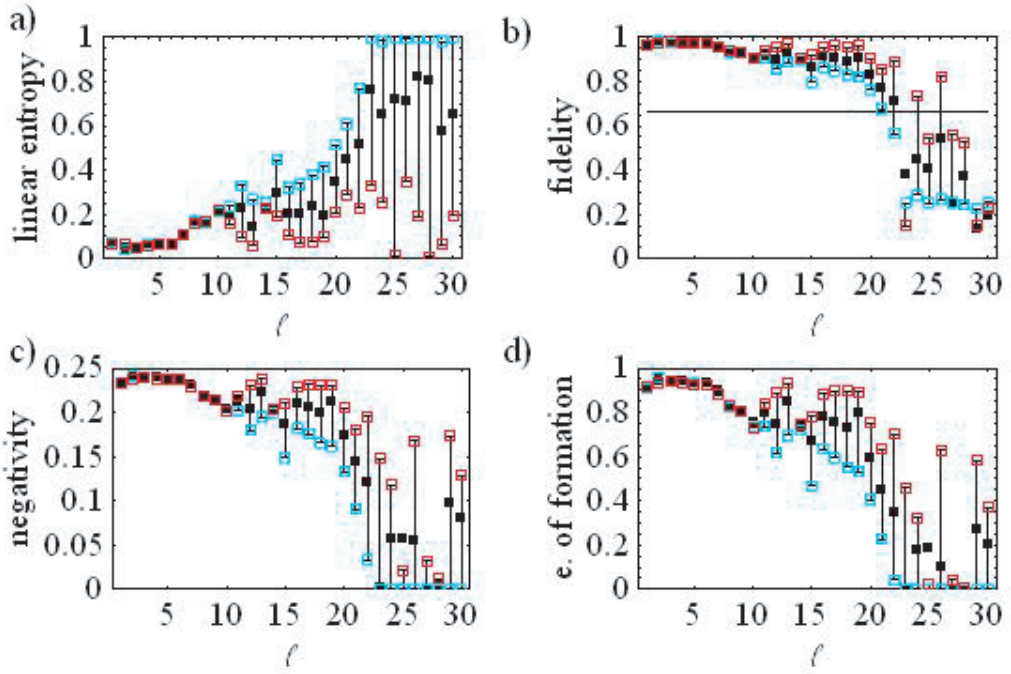

Figure 6. Various measures of state purity and entanglement for OAM subspaces between $|\ell| = 1$ and 30, and the maximum (red) and minimum (cyan) level consistent with the measurements. Horizontal lines indicate the border between entangled and mixed states. Strong entanglement persists up to an OAM of about 20.

also the filtering during the detection process might be less efficient for states with a higher OAM. The very low count-rates for higher OAM states (compare figure 1) means that any sources of noise may dominate the signal.

The fidelity with the target state, the maximally entangled Bell-state Φ_- is given by $F(\rho, \rho_T) \doteq [\mathrm{Tr}(\sqrt{\sqrt{\rho_\mathrm{T}}\rho\sqrt{\rho_\mathrm{T}}})]^2$, where ρ_T is the density matrix of the target state [31]. In our case, the target state is the pure state (4), so the fidelity simplifies to $F = \langle\Psi|\rho|\Psi\rangle$. For OAM subspaces reaching from $|\ell| = 1$ to 20, we find a fidelity in the range of $F = 0.978$ (at $|\ell| = 3$) and $F = 0.826$ (at $|\ell| = 20$) (see figure 6(b)).

5. Measures of entanglement

From the two-photon density matrices we can obtain various measures of entanglement for a wide range of $|\ell|$ subspaces (including negativity, concurrence, tangle and entanglement of formation) [32]. A selection of these is shown in figure 6(c). A state is entangled if it cannot be described as the product state of its subsystems or as an incoherent mixture of such states. This feature can be quantified by evaluating the partial transpose of a two-photon state, transposing only one of the subsystems, and then identifying the eigenvalues of the partial transpose. If the system was a product state, the partial transpose is simply the transpose of one of the subsystems, which is a valid density matrix. If however the system was entangled, the partial transpose exhibits one or more negative eigenvalues. The negativity is defined as half the modulus of the smallest eigenvalue. For a maximally entangled state, the negativity is 0.25

and vanishes for a completely mixed state. For our system, we find the largest negativity of 0.241 for the $|\ell| = 3$ subspace, which decreases to 0.174 at $|\ell| = 20$ and almost vanishes for extremely high OAM subspaces as shown in figure 6(c).

Alternatively, the fidelity with the maximally entangled Bell-state may be taken as a measure of entanglement. A two-photon state cannot be described as the product state of its subsystems if the fidelity with the Bell-state sinks below 2/3. In this sense, entanglement persists in our system up to the OAM subspace $|\ell| = 22$.

The entanglement of formation [7] characterizes the entanglement of a given state by the resources needed to create it. The entanglement of formation $\mathcal{E}$ is expressed as a function of the concurrence C which also is a measure of entanglement. The concurrence is $C(\rho) = \max(0, \lambda_1 - \lambda_2 - \lambda_3 - \lambda_4)$, where λ_i are the eigenvalues, in decreasing order, of the Hermitian matrix $\sqrt{\sqrt{\rho}\bar{\rho}\sqrt{\rho}}$, where $\bar{\rho}$ is obtained from ρ by an effective spin flip (or in our case a flip of OAM) on both of the states [7]. For a maximally entangled state, the concurrence is equal to 1, whereas for an unentangled state it is 0. From our density matrix we calculate a concurrence between $C = 0.969$ and 0.700 (at $|\ell| = 20$). The entanglement of formation is defined as $\mathcal{E} = -x \log_2(x) - (1-x) \log_2(1-x)$, where $x = 1/2(1 + \sqrt{1 - C^2})$, and we find values between 0.956 and 0.591 (see figure 6(d)).

We note that for all measures of entanglement we obtain the largest values for small $|\ell|$ which decrease with $|\ell|$. We observe the largest values for $|\ell| = 3$ which may be explained by the fact that the contribution of higher order sidebands generated by our segment masks are more dominant for the OAM subspaces of $|\ell| = 1$ and 2. The coincidence counts become comparable to the noise background for OAM subspaces of $|\ell| > 22$ and consequently quantum correlations deteriorate towards this cut-off.

6. Conclusions

We have reconstructed density matrices of down-converted photons within a subspace defined by the OAM states $|\pm\ell\rangle$. Our method allows us to estimate the range of entanglement consistent with our measurements. Due to phase-matching during in the down-conversion process, most photons are generated with lower OAM values, with coincidence count-rates dropping to below 10% for $|\ell| = 4$ and below 1% for $|\ell| = 8$ compared to $|\ell| = 1$ in our set-up, nevertheless we find strong entanglement even for photons with OAM far outside of this region up to OAM values of about $\ell = 20$. This gives an indication of the effective dimension of the usable Hilbert space defined by the OAM states that may be utilized in advanced quantum protocols.

Acknowledgments

We thank Monika Ritsch-Marte for valuable discussions. This work is supported by the UK EPSRC, and we acknowledge the financial support of the Future and Emerging Technologies (FET) programme within the Seventh Framework Programme for Research of the European Commission, under the FET open grant agreement HIDEAS, number FP7-ICT-221906. SFA is an RCUK Research Fellow. SMB thanks the Royal Society and the Wolfson Foundation. We would like to thank Hamamatsu for their support of this work.

References

[1] Aspect A, Grangier Ph and Roger G 1981 Experimental tests of realistic local theories via Bell's theorem *Phys. Rev. Lett.* **47** 460

[2] Ekert A K 1991 Quantum cryptography based on Bell theorem *Phys. Rev. Lett.* **67** 661

[3] Simon C and Pan J-W 2002 Polarization entanglement purification using spatial entanglement *Phys. Rev. Lett.* **89** 257901

[4] Guehne O and Toth G 2009 Entanglement detection *Phys. Rep.* **474** 1–75

[5] Fan J, Eisaman M D and Migdall A 2007 Quantum state tomography of a fiber-based source of polarization-entangled photon pairs *Opt. Express* **15** 18339

[6] James D F V, Kwiat P G, Munroe W J and White A G 2001 Measurement of qubits *Phys. Rev.* A **64** 052312

[7] Wootters W K 1998 Entanglement of formation of an arbitrary state of two qubits *Phys. Rev. Lett.* **80** 2245

[8] Einstein A, Podolsky B and Rosen N 1935 Can quantum-mechanical description of physical reality be considered complete? *Phys. Rev.* **47** 777–80

[9] Collins D, Gisin N, Linden N, Massar N and Popescu S 2002 Bell inequalities for arbitrarily high-dimensional systems *Phys. Rev. Lett.* **88** 040404

[10] Leach J, Jack B, Romero J, Ritsch-Marte M, Boyd R W, Jha A K, Barnett S M, Franke-Arnold S and Padgett M J 2009 Violation of a Bell inequality in two-dimensional orbital angular momentum state-spaces *Opt. Express* **17** 8287

[11] Mair A, Vaziri A, Weihs G and Zeilinger A 2001 Entanglement of the orbital angular momentum states of photons *Nature* **412** 313

[12] Barreiro J T, Langford N K, Peters N A and Kwiat P G 2005 Generation of hyperentangled photon pairs *Phys. Rev. Lett.* **95** 260501

[13] Allen L, Padgett M and Babiker M 1999 The orbital angular momentum of light *Prog. Opt.* **39** 291–37
Franke-Arnold S, Padgett M and Allen L 2008 *Laser Photon. Rev.* **2** 299–313

[14] Vaziri A, Weihs G and Zeilinger A 2002 Superpositions of the orbital angular momentum for applications in quantum experiments *J. Opt. B: Quantum Semiclass. Opt.* **4** S47S51

[15] Molina-Terriza G, Torres J P and Torner L 2007 Twisted photons *Nat. Phys.* **75** 305

[16] Franke-Arnold S, Barnett S M, Yao E, Leach J, Courtial J and Padgett M 2004 Uncertainty principle for angular position and angular momentum *New J. Phys.* **6** 103

[17] Molina-Terriza G, Vaziri A, Reháček J, Hradil Z and Zeilinger A 2004 Triggered qutrits for quantum communication protocols *Phys. Rev. Lett.* **92** 167903

[18] Shih Y 2007 Quantum imaging *Quantum IEEE Electron.* **13** 1016

[19] Asbóth J K, Calsamiglia J and Ritsch H 2005 Computable measure of nonclassicality for light *Phys. Rev. Lett.* **94** 173602

[20] Inoue R, Kanai N, Yonehara T, Miyamoto Y, Koashi M and Kozuma M 2006 Entanglement of orbital angular momentum states between an ensemble of cold atoms and a photon *Phys. Rev.* A **74** 053809
Inoue R, Yonehara T, Miyamoto Y, Koashi M and Kozuma M 2009 Measuring qutrit–qutrit entanglement of orbital angular momentum states of an atomic ensemble and a photon *Phys. Rev. Lett.* **103** 110503

[21] Matsukevich D N, Maunz P, Moehring D L, Olmschenk S and Monroe C 2008 Bell inequality violation with two remote atomic qubits *Phys. Rev. Lett.* **100** 150404

[22] Torres J P, Alexandrescu A and Torner Ll 2003 Quantum spiral bandwidth of entangled two-photon states *Phys. Rev.* A **68** 050301R

[23] Franke-Arnold S, Barnett M S, Padgett M J and Allen L 2002 Two photon entanglement of angular momentum states *Phys. Rev.* A **65** 033823

[24] Osorio C I, Molina-Terriza G and Torres J P 2008 Correlations in orbital angular momentum of spatially entangled paired photons generated in parametric down-conversion *Phys. Rev.* A **77** 015810

[25] Barnett S M and Pegg D T 1990 Quantum theory of rotation angles *Phys. Rev.* A **41** 3427
Franke-Arnold S, Barnett M S, Yao E, Leach J, Courtial J and Padgett M J 2004 Uncertainty principle for angular position and angular momentum *New J. Phys.* **6** 103

[26] Jack B, Padgett M J and Franke-Arnold S 2008 Angular diffraction *New J. Phys.* **10** 103013
[27] Ling A, Lamas-Linares A and Kurtsiefer Ch 2008 Accuracy of minimal and optimal qubit tomography for finite-length experiments. arXiv:0807.0991v1
[28] Press W H, Teukolsky S A, Vetterling W T and Flannery B P 1995 *Numerical Recepies in C* 2nd edn (Cambridge: Cambridge University Press) chapter 18
[29] Resch K J, Walther P and Zeilinger A 2005 Full characterization of a three-photon Greenberger–Horne–Zeilinger state using quantum state tomography *Phys. Rev. Lett.* **94** 070402
[30] Langford N K, Dalton R B, Harvey M D, OBrien J L, Pryde G J, Gilchrist A, Bartlett S D and White A G 2004 measuring entangled qutrits and their use for quantum bit commitment *Phys. Rev. Lett.* **93** 053601
[31] Josza R 1994 Fidelity for mixed quantum states *J. Mod. Opt.* **41** 2315
[32] Barnett S M 2009 *Quantum Information* (Oxford: Oxford University Press)